

Cutoff-free Circuit Quantum Electrodynamics

Moein Malekakhlagh, Alexandru Petrescu, and Hakan E. Türeci

Department of Electrical Engineering, Princeton University, Princeton, New Jersey, 08544

(Dated: December 3, 2024)

Any quantum-confined electronic system coupled to the electromagnetic continuum is subject to radiative decay and renormalization of its energy levels. When coupled to a cavity, these quantities can be strongly modified with respect to their values in vacuum. Generally, this modification can be accurately captured by including only the closest resonant mode of the cavity. In the circuit quantum electrodynamics architecture, where the coupling strengths can be substantial, it is however found that the radiative decay rates are strongly influenced by far off-resonant modes. A multimode calculation accounting for the infinite set of cavity modes leads to divergences unless a cutoff is imposed. It has so far not been identified what the source of divergence is. We show here that unless gauge invariance is respected, any attempt at the calculation of circuit QED quantities is bound to diverge. We then present a theoretical approach to the calculation of a finite spontaneous emission rate and the Lamb shift that is free of cutoff.

Introduction. A discrete-level atom-like degree of freedom coupled to the continuum of electromagnetic (EM) modes spontaneously decays. When the atom is confined in a resonator, the emission rate can be suppressed or enhanced with respect to its value in free space, depending on the local density of states of the EM environment at the atomic position [1–4]. This is referred to as the Purcell effect [5]. An accompanying effect of the coupling to the EM vacuum is the Lamb shift, a radiative level shift that was first observed in the microwave spectroscopy of the hydrogen $^2P_{1/2} - ^2S_{1/2}$ transition [6]. These quantities have been experimentally accurately characterized for superconducting Josephson junction (JJ) based qubits coupled to coplanar transmission line [7, 8] and three-dimensional resonators [9]. In the dispersive regime where a qubit with transition frequency ω_j is far detuned from the nearest resonant cavity mode (frequency ω_r , loss κ_r), the Purcell decay rate and the Lamb shift are given by $\gamma_P = (g/\delta)^2 \kappa_r$ and $\Delta_L = g^2/\delta$, respectively. Here g denotes the coupling between the qubit and the cavity mode and $\delta = \omega_j - \omega_r$ their mutual detuning [10]. However for large couplings accessible in circuit quantum electrodynamics, single-mode approximation is often found to be inaccurate [7, 8]. In particular, it has been noted that the qubit relaxation times, when not limited by absorptive losses, are often limited by the EM modes of the circuit that are far detuned from the qubit transition frequency [8]. Similarly the experimentally measured Lamb shift in the dispersive regime can only be accurately fit with an extended Jaynes-Cummings (JC) model including several modes and qubit levels [7]. A generalization of the Purcell rate can be found that accounts for coupling of the qubit to all resonator modes

$$\gamma_P = \sum_n (g_n/\delta_n)^2 \kappa_n, \quad (1)$$

where g_n is the coupling strength of the qubit to mode n and $\delta_n = \omega_j - \omega_n$ is its detuning from the corresponding resonator mode with resonance frequency ω_n and decay rate κ_n . It has been pointed out however that this ex-

pression is divergent unless a cutoff is imposed by hand on the number of modes kept [8]. These divergences are not limited to the Purcell relaxation and the Lamb shift, but appear in other vacuum-induced quantum electrodynamics (QED) phenomena such as photon-mediated qubit-qubit interactions as well [11]. So far no satisfactory theoretical explanation has been given for the source of these divergences. Here we show that, within the framework of circuit quantum electrodynamics as formulated in Ref. [12], finite QED expressions are obtained when gauge invariance is respected. We confine ourselves here to a transmon-type JJ qubit [13] coupled to an open transmission-line resonator, but our results should be valid for other types of open EM environments as well.

Gauge invariance in circuit QED. The role of gauge invariance in the correct accounting for light-matter interactions has been a vexing question since the early days of quantum electrodynamics (see e.g. [14] and the references therein). Since it plays a similarly critical role here, we would like to first expound on the specific meaning of gauge invariance in the context of superconducting electrical circuits, and its impact on QED observables, which to our knowledge has not been satisfactorily addressed before.

As the starting point of our discussion, we consider a transmon-type qubit coupled to a coplanar waveguide resonator that is capacitively coupled at both ends to infinitely long waveguides (Fig. 1a). A convenient but not unique way to describe such electrical quantum circuits assigns a flux variable to each node, given by $\Phi_n(t) = \int^t d\tau V_n(\tau)$, with $V_n(t)$ being the instantaneous voltage at the node n measured with respect to a chosen ground node [12, 15]. The choice of the ground node is analogous to the choice of a particular gauge in the electromagnetic field theory [12]. For the connection geometry with the associated choice of the ground node shown in Fig 1a, the light-matter interaction term derives from the energy on the gate capacitor, given by $T_{\text{int}} = \frac{1}{2} C_g [\dot{\Phi}(x_0) - \dot{\Phi}_j]^2$ in the circuit Lagrangian [16], where x_0 is the connection point of the JJ to the transmission line in the dipole

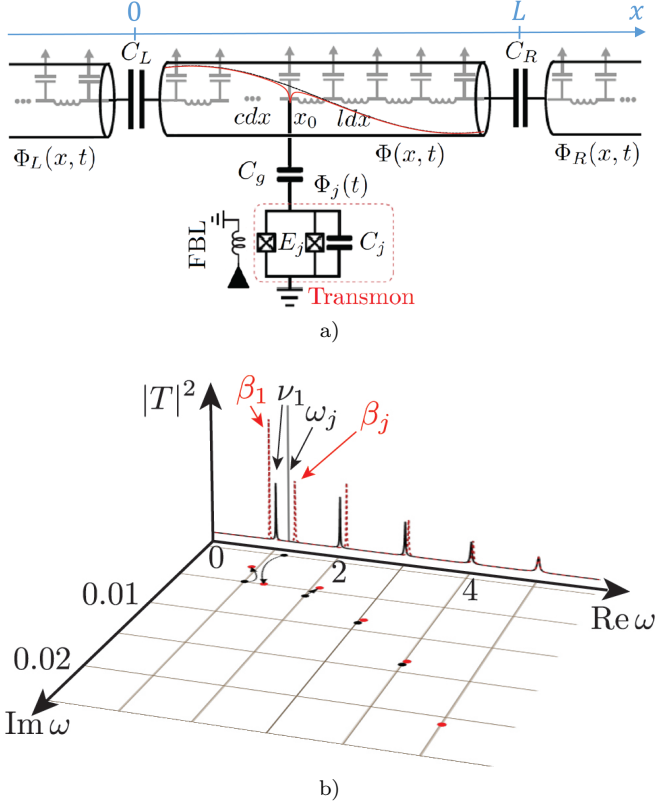


FIG. 1. a) A transmon qubit coupled to an open superconducting resonator. The black dashed line is a cartoon of the fundamental bare mode of the resonator, while the red solid curve represents the modified resonator mode. b) The transmission $|T|^2$ is shown versus the real frequency for the bare resonator modes (solid black curves). Capacitively coupling the qubit, whose transition frequency ω_j is slightly above the fundamental resonator frequency ν_1 , gives rise to hybridized modes (dashed red curves). Alternatively, one may study the positions of these resonances in the complex frequency plane, where the bare resonator and qubit poles (black points) are displaced into hybridized resonator-like and qubit-like resonances (red points). The Purcell decay and the Lamb shift are obtained as the displacement of the qubit-like pole. The bare (hybridized) complex frequencies are the poles (zeros) of the characteristic function $D_j(s)$.

approximation. Among the three terms in its expansion, $T_{\text{EM}} = \frac{1}{2}C_g\dot{\Phi}(x_0)^2$, $T_{\text{EM-JJ}} = -C_g\dot{\Phi}(x_0) \cdot \dot{\Phi}_j$ and $T_{\text{JJ}} = \frac{1}{2}C_g\dot{\Phi}_j^2$, retaining only the direct interaction term $T_{\text{EM-JJ}}$, a multimode JC model can be derived with g_n , ω_n and κ_n expressed in terms of the circuit variables [16], which as pointed out above, gives rise to a diverging expression for a dispersively coupled qubit. In reaching this open JC Model, generally one or more of a number of approximations are done: Truncation of the qubit subsystem to two-levels providing a pseudo-spin description for the JJ, the rotating wave approximation to neglect non-secular terms (such as the counter-rotating terms and other non-resonant transitions of the qubit), and the Born and the Markov approximations to arrive at

a Master equation description to account for losses due to the cavity-waveguide coupling. So far it has not been clarified which of these approximations is behind the divergence or whether the divergence is a fundamental issue to be resolved at higher energies where the effective low-energy field theory provided by the subgap circuit quantum electrodynamics ceases to be valid. As discussed below, retention of only the direct interaction term $T_{\text{EM-JJ}}$ violates gauge invariance. We find that the full accounting of all the terms, in particular the term T_{EM} equivalent to the diamagnetic A^2 term in the minimal coupling Hamiltonian $(p - eA)^2/2m$ [17], makes all the difference between a finite and an infinite result for all of the QED observables that we have studied.

The general line of thought about the impact of the A^2 -term in vacuum-induced effects such as the Lamb shift is that it should have no impact on transition frequencies. Because this term does not involve any atomic operators, it is expected to make the same perturbative contribution to every atomic energy level, and hence should not effect observable shifts in *transition* frequencies [18] (See Sec. 3.4). However this argument is firmly rooted in perturbation theory in the A^2 -term. As we show below, the diamagnetic term *does* have a critical impact when its effect is accounted for exactly, to all orders. This can be done while still keeping the calculations tractable, as we describe below.

Heisenberg equations of motion. The dimensionless Heisenberg equations of motion describing the infinite network shown in Fig. 1a, extending from $x = -\infty$ to $x = \infty$, are [16, 19]

$$\hat{\varphi}_j(t) + (1 - \gamma)\omega_j^2 \sin[\hat{\varphi}_j(t)] = \gamma \partial_t^2 \hat{\varphi}(x_0, t), \quad (2)$$

$$[\partial_x^2 - \chi(x, x_0)\partial_t^2] \hat{\varphi}(x, t) = \chi_s \omega_j^2 \sin[\hat{\varphi}_j(t)] \delta(x - x_0). \quad (3)$$

Here $\hat{\varphi}_j(t)$ and $\hat{\varphi}(x, t)$ are the dimensionless flux operators for the JJ and the cavity-waveguide system, respectively, $\gamma \equiv C_g/(C_g + C_j)$ is a capacitive ratio, $\chi_s = \gamma C_j/cL$ is the dimensionless series capacitance of C_g and C_j , ω_j is the dimensionless transmon frequency. In addition, we define $\chi_i \equiv C_i/(cL)$ for $i = g, j, R, L$ [16]. These two inhomogeneous equations show that the flux field at x_0 drives the dynamics of the JJ (Eq. (2)), while the JJ acts as a source driving the EM fields in the transmission line (Eq. (3)). In addition, the fields are subject to continuity conditions at the ends of the resonator at $x = 0$ and $x = 1$ (in units of L). Physically these continuity conditions amount to current conservation [17], which is consistent with Kirchhoff's laws for the expectation value of the currents in the circuit.

It is interesting to trace the impact of the individual terms in T_{int} in the equations above. T_{JJ} modifies the mass and the frequency of the JJ oscillator (Eq. (2)), renormalizing γ from C_g/C_j to $C_g/(C_g + C_j)$, while the direct interaction term $T_{\text{EM-JJ}}$ is responsible for the appearance of the source terms in both equations. The most critical feature for the discussion here is the impact of T_{EM} . It introduces an effective scattering term in the wave equation describing the fields in the transmission

line, by modifying the unitless capacitance per length from 1 to $\chi(x, x_0) = 1 + \chi_s \delta(x - x_0)$. Similar modification of resonator modes has been pointed out before for JJ-based qubits [9, 17, 20]. We discuss its impact on QED observables below. The satisfaction of gauge-invariance firmly rests on the exact inclusion of these terms in the Heisenberg equations of motion with their correct relative magnitudes.

Equation 3 can be solved in the Fourier domain. The Fourier transform of the transmission line field $\hat{\varphi}(x, \omega) = \int_{-\infty}^{\infty} dt \hat{\varphi}(x, t) e^{-i\omega t}$ can most conveniently be expressed in the basis $\tilde{\varphi}_n(x, \omega)$ that solves the generalized eigenvalue problem $[\partial_x^2 + \chi(x, x_0) \omega^2] \tilde{\varphi}_n(x, \omega) = 0$, subject to continuity conditions at the ends of the resonator, i.e. $-\partial_x \tilde{\varphi}_n(1^-, \omega) = \chi_R \omega^2 [\tilde{\varphi}_n(1^-, \omega) - \tilde{\varphi}_n(1^+, \omega)]$ and $-\partial_x \tilde{\varphi}_n(0^+, \omega) = \chi_L \omega^2 [\tilde{\varphi}_n(0^-, \omega) - \tilde{\varphi}_n(0^+, \omega)]$, which models the coupling to the waveguides and associated loss. The Dirac δ -function in $\chi(x, x_0)$ leads to the discontinuity

$$-\partial_x \tilde{\varphi}_n(x) \Big|_{x_0^-}^{x_0^+} = \chi_s \omega_n^2 \tilde{\varphi}_n(x_0). \quad (4)$$

Physically, this discontinuity condition expresses the current conservation at the node of connection to the qubit, resulting in a modified, current-conserving (CC) basis for the transmission line [17]. These modifications in the spectrum of the transmission line in turn will impact the dynamics of the JJ driven by the resonator fluctuations.

The role of modal modification in Eq. (33) can be illustrated with a phenomenological model. Previously, the Purcell rate and the Lamb shift have been calculated using the Lindblad formalism in the dispersive limit [10]. An effective multimode JC model

$$\hat{\mathcal{H}}_{\text{JC}} = \frac{\omega_j}{2} \hat{\sigma}_z + \sum_n \omega_n \hat{a}_n^\dagger \hat{a}_n + \sum_n g_n (\hat{\sigma}^+ \hat{a}_n + \hat{\sigma}^- \hat{a}_n^\dagger) \quad (5)$$

can be obtained from our first principles model [16], which incorporates the modifications to the resonator modes and the JJ dynamics due to the gauge-invariant form of the interaction. Resonator losses are included by a Bloch-Redfield approach through the zero-temperature Master equation for the reduced density matrix of the resonator and qubit degrees of freedom $\dot{\hat{\rho}} = -i[\hat{\mathcal{H}}_{\text{JC}}, \hat{\rho}] + \frac{\kappa_n}{2} (2\hat{a}_n \hat{\rho} \hat{a}_n^\dagger - \{\hat{\rho}, \hat{a}_n^\dagger \hat{a}_n\})$. The expression of the effective cavity frequencies ω_n , the associated losses κ_n and the modal interaction strengths g_n are given in the Supplementary Material [16]. Interestingly all these quantities are functions of χ_s , a measure of the qubit-resonator coupling, in a significant fashion. We show in Fig. 2a that the interaction strength of the qubit with mode n becomes non-monotonic as soon as χ_s is nonzero, first increasing then turning over at a critical n (that is χ_s dependent), decreasing as $g_n \sim 1/\sqrt{n}$ in the large- n limit, as analytically shown in the Supplementary Material. The decrease in g_n , critical in rendering the multimode Purcell rate finite without an imposed cutoff as discussed below, can be associated with the modification of the resonator modes for $\chi_s \neq 0$ (see Fig. 1b). This phenomenon is not

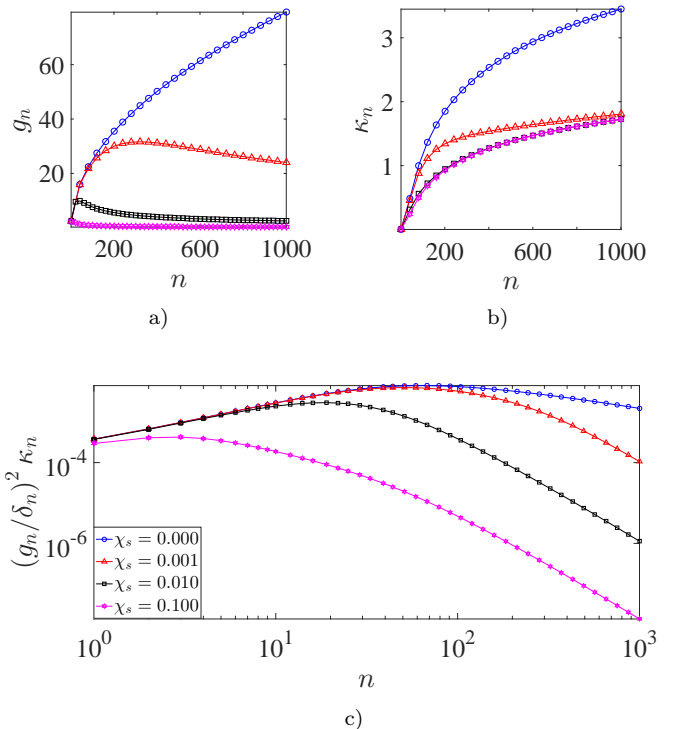


FIG. 2. (Color online) Dependence of a) coupling strength g_n , b) Purcell decay rate in the dispersive regime $(g_n/\delta_n)^2 \kappa_n$ on mode number n for different values of $\chi_s = \{0, 10^{-3}, 10^{-2}, 10^{-1}\}$. Other parameters are set as $\chi_R = \chi_L = 10^{-3}$ and $x_0 = 0^+$.

specific to the chosen resonator geometry in Fig. 1a. The underlying physical reason is the conservation of current at the position of the qubit $x = x_0$, imposed by accounting fully for the gauge invariance of the interaction. In the large frequency limit, the series capacitance χ_s becomes a short-circuit to ground. In other words, χ_s acts as a low-pass filter and hence the mode amplitude vanishes at x_0 for large frequencies. This behavior in turn leads to a power law drop in the magnitude of modal interaction constants g_n as $n \rightarrow \infty$ (Fig. 2a). Moreover, eliminating the continuum degrees of freedom of the attached waveguides results in an effective decay rate for each mode, κ_n which increases monotonically for large n , $\kappa_n \sim n^{0.3}$ (Fig. 2b). In the Supplementary Material, we show that for $\chi_s = 0$ the resulting series Eq. (1) diverges [16], as pointed out in previous studies [8, 11]. For any nonzero χ_s , the asymptotic form of the individual terms in the sum of Eq. (1) attains a universal slope, approximately -2.7 (Fig. 2c), which is strictly less than -1 and therefore convergent [21].

Solution of linearized Heisenberg equations. Although we showed that the expression (1) for the Purcell decay rate is convergent, this estimate is only valid in the dispersive regime where $g_n \ll \delta_n$. The dispersive-regime estimate for the Purcell decay rate and the Lamb shift will deviate substantially from the exact result for a range

of order g_n around each cavity resonance, diverging as the qubit frequency approaches any of the resonance frequencies (see Fig. 3). In addition, this result is obtained in the two-level approximation for the transmon, in the rotating wave approximation for all interactions, and in the Born and Markov approximations for the coupling to the waveguides. These approximations cast an uncertainty about the reliability of the dispersive-limit result Eq. (1) and its convergence, which we address next.

An improved analytic result that is uniformly valid in the transmon frequency, and is not limited by the aforementioned approximations can be found by solving Eqs. (2-3) in a perturbation theory in the transmon nonlinearity. EM degrees of freedom can be fully integrated out by solving Eq. (3) exactly, plugging into Eq. (2) and subsequently tracing over the photonic Hilbert space. To lowest order in the transmon nonlinearity $\epsilon = (E_c/E_j)^{1/2}$, where E_c and E_j are the charging and Josephson energy, respectively, the governing equation is [19]

$$\begin{aligned} \hat{\ddot{X}}_j(t) + \omega_j^2 [1 - \gamma + i\mathcal{K}_1(0)] \hat{X}_j(t) \\ = -\omega_j^2 \int_0^t dt' \mathcal{K}_2(t-t') \hat{X}_j(t'), \end{aligned} \quad (6)$$

where $\hat{X}_j(t) = \text{Tr}_{ph}\{\hat{\rho}_{ph}(0)\hat{\phi}_j(t)\}/\phi_{zpf}$ is the reduced flux operator traced over the photonic degrees of freedom and $\phi_{zpf} \equiv (\sqrt{2}\epsilon)^{1/2}$ is the magnitude of the zero-point fluctuation in the phase. This delay equation features the memory kernels $\mathcal{K}_n(\tau) \equiv \gamma\chi_s \int_{-\infty}^{+\infty} \frac{d\omega}{2\pi} \omega^n G(x_0, x_0, \omega) e^{-i\omega\tau}$, where $G(x, x', \omega)$ is the classical EM Green's function defined by $[\partial_x^2 - \chi(x, x_0)\partial_t^2] G(x, x', \omega) e^{-i\omega t} = e^{-i\omega t} \delta(x - x')$ implying that $G(x, x', \omega)$ is the amplitude of the flux field created at x by a transmon oscillating with a frequency ω at x' [19]. The term on the right hand side of Eq. (7) therefore is proportional to the fluctuating current driving the transmon oscillator at time t , that was excited by itself at an earlier time t' . We note that the propagation of excitations is informed by the modification of the capacitance per length at the transmon connection point, a consequence of enforcing gauge invariance. Eq. (7) can be solved exactly in the Laplace domain

$$\hat{\ddot{X}}_j(s) = \frac{s\hat{X}_j(0) + \hat{X}_j(0)}{D_j(s)}, \quad (7)$$

where $\tilde{h}(s) \equiv \int_0^\infty dt h(t) e^{-st}$, with $D_j(s)$ defined as [19]

$$D_j(s) \equiv s^2 + \omega_j^2 \left[1 - \gamma + i\mathcal{K}_1(0) + \tilde{\mathcal{K}}_2(s) \right]. \quad (8)$$

A convenient and physically transparent representation of $D_j(s)$ can be found in the form

$$D_j(s) = (s - p_j)(s - p_j^*) \prod_m \frac{(s - p_m)(s - p_m^*)}{(s - z_m)(s - z_m^*)}. \quad (9)$$

which manifestly exposes the meromorphic structure of the function $D_j(s)$: the poles of $1/D_j(s)$ are the hybridized transmon-like and cavity-like complex-valued excitation frequencies, $p_j \equiv -\alpha_j - i\beta_j$ and $p_n \equiv -\alpha_n - i\beta_n$, respectively, of the qubit-resonator system, while its zeroes $z_n \equiv -i\omega_n = -\kappa_n - i\nu_n$ correspond to bare non-Hermitian [16] cavity resonances. The relevant information about the Lamb shift and the Purcell decay of the transmon is encoded in the hybridized qubit-like pole p_j ; its real part α_j is the Purcell loss rate, while $\beta_j - \omega_j$ is the Lamb shift, which is shown schematically in Fig. 1b. In the Supplementary Material, we show that these physical observables diverge if we employ unmodified resonator modes ($\chi_s = 0$ on the left hand side of Eq. (3)) [16]. The divergence is more general: $D_j(s)$ for any s is divergent and hence all the hybridized resonances are shifted by an infinite amount. In contrast, we show convergence for these physical observables and more generally for the entire $D_j(s)$ for any nonzero χ_s , even if infinitesimal. The A^2 term kept in our calculation to enforce gauge invariance plays the role of the ‘‘counterterm’’ discussed by Caldeira and Leggett [22, 23], which is generally added by hand to cancel the infinite renormalization of frequencies in a field theory of coupled modes. This problem was encountered early on in the formulation of the quantum theory of laser radiation [24]. The addition of the counterterm is analogous to mass renormalization in quantum electrodynamics [25]. Our microscopic gauge-invariant theory includes the counterterm from the beginning, and its effect is accounted for exactly, to all orders in perturbation theory.

Perturbative corrections. The transmon nonlinearity neglected in Eq. (7) can be reintroduced as a weak perturbation to the exactly solvable linear theory. The leading order correction to the hybridized resonances amounts to self- and cross-Kerr interactions [9, 20]. Using multi-scale perturbation theory [19, 26], the correction to β_j is given by

$$\hat{\beta}_j = \beta_j - \frac{\sqrt{2}\epsilon}{4} \omega_j \left[u_j^4 \hat{\mathcal{H}}_j(0) + \sum_n u_j^2 u_n^2 \hat{\mathcal{H}}_n(0) \right] \quad (10)$$

where the coefficients $u_{j,n}$ define the transformation from the hybridized to the unhybridized modes and $\hat{\mathcal{H}}_{j,n}(0)$ are the free Hamiltonian of the transmon and mode n , respectively. For $\chi_g \rightarrow 0$, we find $u_j \rightarrow 1$, $u_n = 0$ and $\beta_j \rightarrow \omega_j$ such that we recover the frequency correction of free quantum Duffing oscillator $\hat{\omega}_j = \omega_j [1 - \frac{\sqrt{2}\epsilon}{4} \hat{\mathcal{H}}_j(0)]$ [27]. We note three features of this result. Firstly, the correction is an operator and that expresses the fact that transmon levels are anharmonic. The anharmonicity can be calculated from the expectation value of a corrected quadrature operator [16]. Secondly, by virtue of the lowest order result being convergent without a cut-off, the perturbative corrections are also convergent in the number of modes included. Finally, this result is not limited by the qubit-resonator coupling strength (as parametrized here by χ_s) or the openness of the cav-

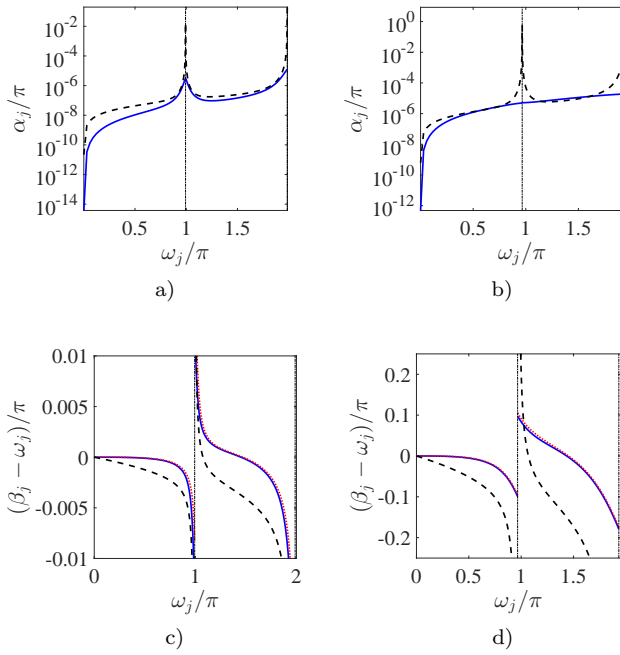


FIG. 3. (Color online) a,b) Comparison of the spontaneous decay rate between the linear theory (blue solid) and the dispersive limit result γ_P (black dashed) as a function of ω_j . c,d) Comparison of the Lamb shift between the linear theory (blue solid), leading order perturbation (red dotted) and the dispersive limit result Δ_L (black dashed). a,c) $\chi_g = 0.001$ and b,d) $\chi_g = 0.1$. The nonlinearity is set as $\epsilon = 0.1$, while other parameters are $\chi_R = \chi_L = 10^{-3}$ and $\chi_j = 0.05$. The vertical dash-dotted black line shows the position of the fundamental frequency of the resonator.

ity (as parametrized by $\chi_{R,L}$). The final result is finite for all qubit frequencies (i.e. for all detunings from cavity resonances), as opposed to the dispersive-limit result discussed earlier. The correction to the Purcell decay is higher order and forms the subject of future work.

We compared the spontaneous decay from the linear theory (solid blue) to the dispersive limit estimate γ_P in Eq. (1)(red dotted) as the transmon frequency is tuned across the fundamental mode in Figs. 3a-3b. The frequency of transmon can be tuned *in situ* by varying the Josephson energy E_j via an external flux [28]. First, the spontaneous decay is asymmetric, since there are (in)finitely many modes with frequency (larger) smaller than ω_j . This feature is captured by both theories. Second, it is enhanced as the frequency of the transmon gets closer to the fundamental frequency of the resonator as expected. However, the dispersive limit estimate is perturbative in g_n/δ_n and hence yields a divergent result at resonance as opposed to the result obtained from Eq. (7).

In Figs. 3c-3d we compare the Lamb shift from the linear theory (blue solid) and the leading order perturbation (red dotted) to the dispersive multimode estimate (black dashed) $\sum_n g_n^2/\delta_n$ [10]. Below the fundamental mode, the Lamb shift is negative due to the collective influence

of all higher modes that tends to redshift the transmon frequency. Above the fundamental mode, there appears a competition between the hybridization with the fundamental mode and all higher modes. Close enough to the fundamental mode, the Lamb shift is positive until it changes sign as predicted by all three curves.

Conclusion. We have presented a framework to calculate the spontaneous decay and the Lamb shift of a transmon qubit, which are convergent in the number of resonator modes without the need for rotating-wave or Markov approximations or a high frequency cutoff. This is achieved by an *ab initio* derivation of the quantum circuit equations of motion with the A^2 term built in, to enforce gauge invariance at all orders consistently. As a result, the modes of the resonator are modified such that the light-matter coupling is suppressed at high frequencies. Formulating the cavity resonances in terms of non-Hermitian modes provides access to the spontaneous decay, the Lamb shift and any other QED observables, in a unified way.

Acknowledgements. We acknowledge helpful discussions with Zlatko Minev and Steven Girvin. This work was supported by the U.S. Army Research Office (ARO) under Grant No. W911NF-15-1-0299.

Note. While finishing this manuscript we became aware of Ref. 29, which arrives at a similar conclusion for the Lamb shift in the dispersive regime through a different approach.

Supplementary Material: Cutoff-free Circuit Quantum Electrodynamics

I. HEISENBERG EQUATIONS OF MOTION

In the following, we use the convention of working with flux variables [15, 30] as the generalized coordinate for our system. For an arbitrary node n in the circuit, the flux variable $\Phi_n(t)$ is defined as

$$\Phi_n(t) \equiv \int_0^t dt' V_n(t'), \quad (11)$$

while $V_n(t')$ stands for the voltage at node n . The classical Lagrangian for the system can be found as sum of the Lagrangians for the Josephson junction, resonator, right and left waveguides, capacitive coupling between the resonator and the waveguides and the transmon-resonator capacitive coupling, respectively:

$$\begin{aligned} \mathcal{L} = & \underbrace{\frac{1}{2} C_j \dot{\Phi}_j(t)^2 - U_j(\Phi_j(t))}_{\mathcal{L}_j} \\ & + \underbrace{\int_{0^+}^{L^-} dx \left[\frac{1}{2} c(\partial_t \Phi)^2 - \frac{1}{2l} (\partial_t \Phi)^2 \right]}_{\mathcal{L}_{\text{Res}}} \\ & + \underbrace{\int_{L^+}^{\infty} dx \left[\frac{1}{2} c(\partial_t \Phi_R)^2 - \frac{1}{2l} (\partial_x \Phi_R)^2 \right]}_{\mathcal{L}_{\text{RW}}} \\ & + \underbrace{\int_{-\infty}^{0^-} dx \left[\frac{1}{2} c(\partial_t \Phi_L)^2 - \frac{1}{2l} (\partial_x \Phi_L)^2 \right]}_{\mathcal{L}_{\text{LW}}} \\ & + \underbrace{\frac{1}{2} C_L \left[\dot{\Phi}_L(0^-, t) - \dot{\Phi}(0^+, t) \right]^2}_{\mathcal{L}_{C_L}} \\ & + \underbrace{\frac{1}{2} C_R \left[\dot{\Phi}_R(L^+, t) - \dot{\Phi}(L^-, t) \right]^2}_{\mathcal{L}_{C_R}} \\ & + \underbrace{\frac{1}{2} C_g \left[\dot{\Phi}_j(t) - \dot{\Phi}(x_0, t) \right]^2}_{\mathcal{L}_{C_g}}, \end{aligned} \quad (12)$$

The classical Euler-Lagrange equations of motion can then be found by setting the variation of Lagrangian with respect to each flux variable to zero. For the transmon and the resonator we find

$$\ddot{\Phi}_j + \frac{1}{C_g + C_j} \frac{\partial U_j(\Phi_j)}{\partial \Phi_j} = \gamma \partial_t^2 \Phi(x_0, t), \quad (13)$$

$$\partial_x^2 \Phi(x, t) - lc(x, x_0) \partial_t^2 \Phi(x, t) = l\gamma \delta(x - x_0) \frac{\partial U_j(\Phi_j)}{\partial \Phi_j}. \quad (14)$$

where $U_j(\Phi_j)$ stands for the Josephson potential as

$$U_j(\Phi_j) = -E_j \cos \left(\frac{2\pi}{\Phi_0} \Phi_j \right), \quad (15)$$

and $\Phi_0 \equiv \frac{h}{2e}$ is the superconducting flux quantum and E_j is the Josephson energy. Furthermore, $C_s \equiv C_g C_j / (C_g + C_j)$ is the series capacitance of C_j and C_g and $\gamma \equiv C_g / (C_g + C_j)$. Moreover, l and c are the inductance and capacitance per length of the resonator and waveguides while $c(x, x_0) \equiv c + C_s \delta(x - x_0)$ represents the modified capacitance per length due to coupling to the transmon located at x_0 .

In addition, we find two wave equations for the flux field of the left and right waveguides as

$$\partial_x^2 \Phi_{R,L}(x, t) - lc \partial_t^2 \Phi_{R,L}(x, t) = 0, \quad (16)$$

The boundary conditions (BC) are derived from continuity of current at each end as

$$\begin{aligned} -\frac{1}{l} \partial_x \Phi|_{x=L^-} &= -\frac{1}{l} \partial_x \Phi_R|_{x=L^+} \\ &= C_R \partial_t^2 [\Phi(L^-, t) - \hat{\Phi}_R(L^+, t)], \end{aligned} \quad (17a)$$

$$-\frac{1}{l} \partial_x \Phi|_{x=0^+} = -\frac{1}{l} \partial_x \Phi_L|_{x=0^-} \quad (17b)$$

$$= C_L \partial_t^2 [\Phi_L(0^-, t) - \Phi(0^+, t)], \quad (17c)$$

continuity of flux at $x = x_0$

$$\Phi(x = x_0^-, t) = \Phi(x = x_0^+, t), \quad (18)$$

and conservation of current at $x = x_0$ which can be obtained from integrating Eq. (14) in the interval $[x_0^-, x_0^+]$ as

$$\partial_x \Phi|_{x=x_0^+} - \partial_x \Phi|_{x=x_0^-} - l C_s \partial_t^2 \Phi(x_0, t) = l\gamma \frac{\partial U_j(\Phi_j)}{\partial \Phi_j}. \quad (19)$$

In order to find the quantum equations of motion, we follow the common procedure of canonical quantization [12, 15, 31]:

- 1) Find the conjugate momenta $Q_n \equiv \frac{\delta \mathcal{L}}{\delta \dot{\Phi}_n}$
- 2) Find the classical Hamiltonian via a Legendre transformation as $\mathcal{H} = \sum_n Q_n \dot{\Phi}_n - \mathcal{L}$
- 3) Find the Hamiltonian operator by promoting the classical conjugate variables to quantum operators such that $\{\hat{\Phi}_m, \hat{Q}_n\} = \delta_{mn} \rightarrow [\hat{\Phi}_m, \hat{Q}_n] = i\hbar \delta_{mn}$. We use a hat-notation to distinguish operators from classical variables.

The derivation for the quantum Hamiltonian of the closed version of this system where $C_{R,L} \rightarrow 0$ can be found in [17] (see App. A, B, and C). Note that

nonzero end capacitors $C_{R,L}$ leave the equations of motion for the resonator and waveguides unchanged, but modify the BC of the problem at $x = 0, L$. The resulting equations of motion for the quantum flux operators $\hat{\Phi}_j$, $\hat{\Phi}(x, t)$ and $\hat{\Phi}_{R,L}(x, t)$ have the exact same form as the classical Euler-Lagrange equations of motion.

Next, we define unitless parameters and variables as

$$\begin{aligned} x &\rightarrow \frac{x}{L}, \quad t \rightarrow \frac{t}{\frac{L}{v_p}}, \quad \omega \rightarrow \frac{\omega}{v_p} L, \\ \hat{\varphi} &\equiv 2\pi \frac{\hat{\Phi}}{\Phi_0}, \quad \hat{n} \equiv \frac{\hat{Q}}{2e} \end{aligned} \quad (20)$$

where $v_p \equiv 1/\sqrt{lc}$ is the phase velocity of the resonator and waveguides. Note that $\hat{\varphi}$ and \hat{n} now represent phase and number operators and satisfy $[\hat{\varphi}_j, \hat{n}_j] = i$ and $[\hat{\varphi}(x, t), \hat{n}(x', t')] = i\delta(x - x')\delta(t - t')$. Furthermore, we define unitless capacitances as

$$\chi_i \equiv \frac{C_i}{cL}, \quad i = R, L, j, g, s \quad (21)$$

as well as a unitless modified capacitance per length as

$$\chi(x, x_0) \equiv 1 + \chi_s \delta(x - x_0). \quad (22)$$

Then, the unitless equations of motion for our system are found as

$$\hat{\varphi}_j(t) + (1 - \gamma)\omega_j^2 \sin[\hat{\varphi}_j(t)] = \gamma \partial_t^2 \hat{\varphi}(x_0, t), \quad (23a)$$

$$[\partial_x^2 - \chi(x, x_0) \partial_t^2] \hat{\varphi}(x, t) = \chi_s \omega_j^2 \sin[\varphi_j(t)] \delta(x - x_0), \quad (23b)$$

$$\partial_x^2 \hat{\varphi}_{R,L}(x, t) - \partial_t^2 \hat{\varphi}_{R,L}(x, t) = 0, \quad (23c)$$

with the unitless BCs given as

$$\begin{aligned} -\partial_x \hat{\varphi}|_{x=1^-} &= -\partial_x \hat{\varphi}_R|_{x=1^-} \\ &= \chi_R \partial_t^2 [\hat{\varphi}(1^-, t) - \hat{\varphi}_R(1^+, t)], \end{aligned} \quad (24a)$$

$$\begin{aligned} -\partial_x \hat{\varphi}|_{x=0^+} &= -\partial_x \hat{\varphi}_L|_{x=0^-} \\ &= \chi_L \partial_t^2 [\hat{\varphi}_L(0^-, t) - \hat{\varphi}(0^+, t)], \end{aligned} \quad (24b)$$

$$\hat{\varphi}(x = x_0^-, t) = \hat{\varphi}(x = x_0^+, t), \quad (24c)$$

$$\begin{aligned} \partial_x \hat{\varphi}|_{x=x_0^+} - \partial_x \hat{\varphi}|_{x=x_0^-} - \chi_s \partial_t^2 \hat{\varphi}(x_0, t) \\ = \chi_s \omega_j^2 \sin[\varphi_j(t)]. \end{aligned} \quad (24d)$$

In Eqs. (23a) and (23b), we have defined the unitless oscillation frequency ω_j as

$$\omega_j^2 \rightarrow lcL^2 \frac{E_j}{C_j} \left(\frac{2\pi}{\Phi_0} \right)^2 = 8\mathcal{E}_c \mathcal{E}_j, \quad (25)$$

where \mathcal{E}_c and \mathcal{E}_j stand for the unitless charging and Josephson energy given as

$$\mathcal{E}_{j,c} \equiv \sqrt{lcL} \frac{E_{j,c}}{\hbar}, \quad (26)$$

with $E_c \equiv \frac{e^2}{2C_j}$. Equations (23a-23b) are Eqs. (2-3) in the main text.

II. SPECTRAL REPRESENTATION OF THE GREEN'S FUNCTION

In order to find the effective dynamics of the transmon qubit, one has to solve for the flux field $\hat{\varphi}(x, t)$ and substitute the result back into the RHS of time evolution of the qubit given by Eq. (23a). It is possible to perform this procedure in terms of the resonator Green's function.

A. Definition of $G(x, t|x', t')$

The resonator Green's function is defined as the response of the linear system of Eqs. (23b-23c) to a δ -function source in space-time as

$$[\partial_x^2 - \chi(x, x_0) \partial_t^2] G(x, t|x_0, t_0) = \delta(x - x_0) \delta(t - t_0), \quad (27)$$

with the same BCs as Eqs. (24a-24c). Using the Fourier transform conventions

$$\tilde{G}(x, x_0, \omega) = \int_{-\infty}^{\infty} dt G(x, t|x_0, t_0) e^{i\omega(t-t_0)}, \quad (28a)$$

$$G(x, t|x_0, t_0) = \int_{-\infty}^{\infty} \frac{d\omega}{2\pi} \tilde{G}(x, x_0, \omega) e^{-i\omega(t-t_0)}, \quad (28b)$$

Eq. (27) transforms into a Helmholtz equation

$$[\partial_x^2 + \omega^2 \chi(x, x_0)] \tilde{G}(x, x_0, \omega) = \delta(x - x_0). \quad (29)$$

Moreover, the BCs are transformed by replacing $\partial_t \rightarrow -i\omega$ as

$$\tilde{G}\Big|_{x=x_0^+} = \tilde{G}\Big|_{x=x_0^-}, \quad (30a)$$

$$\partial_x \tilde{G}\Big|_{x=x_0^+} - \partial_x \tilde{G}\Big|_{x=x_0^-} + \chi_s \omega^2 \tilde{G}\Big|_{x=x_0} = 1, \quad (30b)$$

$$\begin{aligned} \partial_x \tilde{G}\Big|_{x=1^-} &= \partial_x \tilde{G}\Big|_{x=1^+} \\ &= \chi_R \omega^2 \left(\tilde{G}\Big|_{x=1^-} - \tilde{G}\Big|_{x=1^+} \right), \end{aligned} \quad (30c)$$

$$\begin{aligned} \partial_x \tilde{G}\Big|_{x=0^-} &= \partial_x \tilde{G}\Big|_{x=0^+} \\ &= \chi_L \omega^2 \left(\tilde{G}\Big|_{x=0^-} - \tilde{G}\Big|_{x=0^+} \right). \end{aligned} \quad (30d)$$

Note that BCs (30a-30d) do not specify what happens to $\tilde{G}(x, x_0, \omega)$ at $x \rightarrow \pm\infty$. We model the baths by imposing outgoing BCs at infinity as

$$\partial_x \tilde{G}(x, x_0, \omega)\Big|_{x \rightarrow \pm\infty} = \pm i\omega \tilde{G}(x \rightarrow \pm\infty, x_0, \omega), \quad (31)$$

which precludes any reflections from the waveguides to the resonator.

B. Spectral representation of Green's function for a closed resonator

It is helpful to revisit spectral representation of Green's function for the closed version of our system by setting $\chi_R = \chi_L = 0$. This imposes Neumann BC $\partial_x \tilde{G}|_{x=0,1} = 0$ and the resulting differential operator becomes Hermitian. The idea of spectral representation is to expand \tilde{G} in terms of a discrete set of normal modes that obey the homogeneous wave equation

$$\partial_x^2 \tilde{\varphi}_n(x) + \chi(x, x_0) \omega_n^2 \tilde{\varphi}_n(x) = 0, \quad (32a)$$

$$\partial_x \tilde{\varphi}_n(x)|_{x=0,1} = 0. \quad (32b)$$

Note that the Dirac δ -function in $\chi(x, x_0)$ leads to the discontinuity

$$-\partial_x \tilde{\varphi}_n(x)|_{x_0^-}^{x_0^+} = \chi_s \omega_n^2 \tilde{\varphi}_n(x_0), \quad (33)$$

which is consistent with the conservation of current at the point of connection to the transmon. This amounts to a suppression of mode amplitude at x_0 . We call this set of eigenmodes the *current-conserving (CC) basis*. The real valued eigenfrequencies obey the transcendental equation

$$\sin(\omega_n) + \chi_s \omega_n \cos(\omega_n x_0) \cos[\omega_n(1-x_0)] = 0. \quad (34)$$

The eigenfunctions read

$$\tilde{\varphi}_n(x) \propto \begin{cases} \cos[\omega_n(1-x_0)] \cos(\omega_n x), & 0 < x < x_0 \\ \cos(\omega_n x_0) \cos[\omega_n(1-x)], & x_0 < x < 1 \end{cases} \quad (35)$$

where the normalization is fixed by the orthogonality condition

$$\int_0^1 dx \chi(x, x_0) \tilde{\varphi}_m(x) \tilde{\varphi}_n(x) = \delta_{mn}. \quad (36)$$

Note that eigenfunctions of a Hermitian differential operator form a complete orthonormal basis. This allows us to deduce the spectral representation of $\tilde{G}(x, x', \omega)$

[32–34] as

$$\tilde{G}(x, x', \omega) = \sum_{n \in \mathbb{N}} \frac{\tilde{\varphi}_n(x) \tilde{\varphi}_n(x')}{\omega^2 - \omega_n^2} = \sum_{\substack{n \in \mathbb{Z} \\ n \neq 0}} \frac{1}{2\omega} \frac{\tilde{\varphi}_n(x) \tilde{\varphi}_n(x')}{\omega - \omega_n}, \quad (37)$$

where the second representation is written due to relations $\omega_{-n} = -\omega_n$ and $\tilde{\varphi}_{-n}(x) = \tilde{\varphi}_n(x)$.

C. Spectral representation of Green's function for an open resonator

A spectral representation can also be found for the Green's function of an open resonator in terms of a discrete set of non-Hermitian modes that carry a constant flux away from the resonator. The Constant Flux (CF) modes [35] have allowed a consistent formulation of the semiclassical laser theory for complex media such as random lasers [36]. The non-Hermiticity originates from the fact that the waveguides are assumed to be infinitely long, hence no radiation that is emitted from the resonator to the waveguides can be reflected back. This results in discrete and complex-valued poles of the Green's function. The CF modes satisfy the same homogeneous wave equation

$$\partial_x^2 \tilde{\varphi}_n(x, \omega) + \chi(x, x_0) \omega_n^2(\omega) \tilde{\varphi}_n(x, \omega) = 0, \quad (38)$$

but with open BCs the same as Eqs. (30a-31). Note that the resulting CF modes $\tilde{\varphi}_n(x, \omega)$ and eigenfrequencies $\omega_n(\omega)$ parametrically depend on the source frequency ω .

Considering only an outgoing plane wave solution for the left and right waveguides based on (31), the general solution for $\tilde{\varphi}_n(x, \omega)$ reads

$$\tilde{\varphi}_n(x, \omega) = \begin{cases} A_n^< e^{i\omega_n(\omega)x} + B_n^< e^{-i\omega_n(\omega)x}, & 0 < x < x_0 \\ A_n^> e^{i\omega_n(\omega)x} + B_n^> e^{-i\omega_n(\omega)x}, & x_0 < x < 1 \\ C_n e^{i\omega x}, & x > 1 \\ D_n e^{-i\omega x}, & x < 0 \end{cases} \quad (39)$$

Applying BCs (30a-30d) leads to a characteristic equation

$$\begin{aligned}
& \sin[\omega_n(\omega)] + (\chi_R + \chi_L)\omega_n(\omega) \left\{ \cos[\omega_n(\omega)] - \frac{\omega_n(\omega)}{\omega} \sin[\omega_n(\omega)] \right\} \\
& - \chi_R \chi_L \omega_n^2(\omega) \left\{ 2i \frac{\omega_n(\omega)}{\omega} \cos[\omega_n(\omega)] + \left[1 + \frac{\omega_n^2(\omega)}{\omega^2} \right] \sin[\omega_n(\omega)] \right\} \\
& + \chi_s \omega_n(\omega) \left\{ \cos[\omega_n(\omega)x_0] - \chi_L \frac{\omega_n(\omega)}{\omega} \{i\omega_n(\omega) \cos[\omega_n(\omega)x_0] + \omega \sin[\omega_n(\omega)x_0]\} \right\} \\
& \times \left\{ \cos[\omega_n(\omega)(1-x_0)] - \chi_R \frac{\omega_n(\omega)}{\omega} \{i\omega_n(\omega) \cos[\omega_n(\omega)(1-x_0)] + \omega \sin[\omega_n(\omega)(1-x_0)]\} \right\} = 0,
\end{aligned} \tag{40}$$

which gives the parametric dependence of CF frequencies on ω . Then, the CF modes $\tilde{\varphi}_n(x, \omega)$ are calculated as

$$\tilde{\varphi}_n(x, \omega) \propto \begin{cases} e^{-i\omega_n(\omega)(x-x_0+1)} [e^{2i\omega_n(\omega)x} + (1 - 2i\omega_n(\omega)\chi_L)] [e^{2i\omega_n(\omega)(1-x_0)} + (1 - 2i\omega_n(\omega)\chi_R)], & 0 < x < x_0 \\ e^{-i\omega_n(\omega)(x_0-x+1)} [e^{2i\omega_n(\omega)x_0} + (1 - 2i\omega_n(\omega)\chi_L)] [e^{2i\omega_n(\omega)(1-x)} + (1 - 2i\omega_n(\omega)\chi_R)], & x_0 < x < 1 \\ -2i\chi_R \omega_n(\omega) e^{-i\omega_n(\omega)(1+x_0)} [e^{+2i\omega_n(\omega)x_0} + (1 - 2i\chi_L \omega_n(\omega))] e^{+i\omega x}, & x > 1 \\ -2i\chi_L \omega_n(\omega) e^{-i\omega_n(\omega)(1-x_0)} [e^{2i\omega_n(\omega)(1-x_0)} + (1 - 2i\chi_R \omega_n(\omega))] e^{-i\omega x}. & x < 0 \end{cases} \tag{41}$$

These modes satisfy the biorthonormality condition

$$\int_0^1 dx \chi(x, x_0) \bar{\tilde{\varphi}}_m^*(x, \omega) \tilde{\varphi}_n(x, \omega) = \delta_{mn}, \tag{42}$$

where $\{\bar{\tilde{\varphi}}_m(x, \omega)\}$ satisfy the Hermitian adjoint of eigenvalue problem (38). In other words, $\tilde{\varphi}_n(x, \omega)$ and $\bar{\tilde{\varphi}}_n(x, \omega)$ are the right and left eigenfunctions and obey $\tilde{\varphi}_n(x, \omega) = \bar{\tilde{\varphi}}_n^*(x, \omega)$. The normalization of Eq. (41) is then fixed by setting $m = n$.

In terms of the CF modes, the spectral representation of the Green's function can then be constructed

$$\tilde{G}(x, x', \omega) = \sum_n \frac{\tilde{\varphi}_n(x, \omega) \bar{\tilde{\varphi}}_n^*(x', \omega)}{\omega^2 - \omega_n^2(\omega)}. \tag{43}$$

Examining Eq. (43), we realize that there are two sets of poles of $\tilde{G}(x, x', \omega)$ in the complex ω plane. First, from setting the denominator of Eq. (43) to zero which gives $\omega = \omega_n(\omega)$. These are the quasi-bound eigenfrequencies that satisfy the transcendental characteristic equation

$$\begin{aligned}
& [e^{2i\omega_n} - (1 - 2i\chi_L \omega_n)(1 - 2i\chi_R \omega_n)] \\
& + \frac{i}{2} \chi_s \omega_n [e^{2i\omega_n x_0} + (1 - 2i\chi_L \omega_n)] \\
& \times [e^{2i\omega_n(1-x_0)} + (1 - 2i\chi_R \omega_n)] = 0.
\end{aligned} \tag{44}$$

The quasi bound solutions ω_n to Eq. (44) reside in the lower half of complex ω -plane and come in symmetric pairs with respect to the $\Im\{\omega\}$ axis, i.e. both ω_n and $-\omega_n^*$ satisfy the transcendental Eq. (44). Therefore, we can label the eigenfrequencies as

$$\omega_n = \begin{cases} -i\kappa_0, & n = 0 \\ +\nu_n - i\kappa_n, & n \in +\mathbb{N} \\ -\nu_n - i\kappa_n, & n \in -\mathbb{N} \end{cases} \tag{45}$$

where ν_n and κ_n are positive quantities representing the oscillation frequency and decay rate of each quasi-bound mode. Second, there is an extra pole at $\omega = 0$ which comes from the ω -dependence of CF states $\tilde{\varphi}_n(x, \omega)$. κ_n is plotted in Fig. (2) of the main text.

III. MULTIMODE JAYNES-CUMMINGS HAMILTONIAN

The classical Hamiltonian for the cQED system can be found from the circuit Lagrangian (12) [17]

$$\begin{aligned}
\mathcal{H}_{sys} = & 4\mathcal{E}_c n_j^2(t) - \mathcal{E}_j \cos[\varphi_j(t)] \\
& + \int_0^1 dx \left\{ \frac{n^2(x, t)}{2\chi(x, x_0)} + \frac{1}{2} [\partial_x \varphi(x, t)]^2 \right\} \\
& + 2\pi\gamma z n_j(t) \int_0^1 dx \frac{n(x, t)}{\chi(x, x_0)} \delta(x - x_0),
\end{aligned} \tag{46}$$

where $z \equiv Z/R_Q$ where $Z \equiv \sqrt{l/c}$ is the characteristic impedance of the resonator and $R_Q \equiv h/(2e)^2$ is the superconducting resistance quantum. The modification in capacitance per length originates from the system Lagrangian that contains the gauge-invariant qubit-resonator coupling $\chi_g [\dot{\varphi}_j(t) - \dot{\varphi}(x_0, t)]^2/2$. In contrast, a phenomenological product coupling $\chi_g \dot{\varphi}_j(t) \dot{\varphi}(x_0, t)$ would yield a \mathcal{H}_{sys} with $\chi_s = 0$ which results in bare resonator modes.

For the purpose of quantizing \mathcal{H}_{sys} , we find the spectrum of the resonator by solving the corresponding Helmholtz eigenvalue problem that has been discussed in Sec. (II B). We find

$$\begin{aligned}\hat{\mathcal{H}}_{\text{sys}} &\equiv \frac{\omega_j}{4} \left\{ \hat{\mathcal{Y}}_j^2 - \frac{\sqrt{2}}{\epsilon} \cos \left[(2\epsilon^2)^{1/4} \hat{\mathcal{X}}_j \right] \right\} \\ &+ \sum_n \left\{ \frac{\omega_n}{4} \left[\hat{\mathcal{X}}_n^2 + \hat{\mathcal{Y}}_n^2 \right] + g_n \hat{\mathcal{Y}}_j \hat{\mathcal{Y}}_n \right\},\end{aligned}\quad (47)$$

where we have defined the canonically conjugate variables $\hat{\mathcal{X}}_l \equiv (\hat{a}_l + \hat{a}_l^\dagger)$ and $\hat{\mathcal{Y}}_l \equiv -i(\hat{a}_l - \hat{a}_l^\dagger)$, where \hat{a}_l represent the boson annihilation operator of sector $l \equiv j, c$. Moreover, $\omega_j \equiv \sqrt{8\mathcal{E}_j\mathcal{E}_c}$ and $\epsilon \equiv \sqrt{\mathcal{E}_c/\mathcal{E}_j}$ is a measure for the strength of transmon nonlinearity. For $\epsilon = 0$, we recover $\omega_j(\hat{\mathcal{X}}_j^2 + \hat{\mathcal{Y}}_j^2)/4$, the Hamiltonian of a simple harmonic oscillator. In the transmon regime where $\epsilon \ll 1$, the leading contribution is $-\sqrt{2}\epsilon\omega_j\hat{\mathcal{X}}_j^4/48$. The coupling between qubit and the n th CC mode of the resonator is

$$g_n = \frac{1}{2}\gamma\sqrt{\chi_j}\sqrt{\omega_j\omega_n}\tilde{\varphi}_n(x_0). \quad (48)$$

There are typically two approaches to diagonalize Eq. (47). In the first approach, assuming that the qubit nonlinearity is strong, one performs a two level reduction. Then, the multimode Rabi Hamiltonian can be derived from Eq. (47) by projecting the quadratures to Pauli sigma matrices, $\hat{\mathcal{X}}_j \rightarrow \hat{\sigma}^x$ and $\hat{\mathcal{Y}}_j \rightarrow \hat{\sigma}^y$, which yields

$$\begin{aligned}\hat{\mathcal{H}}_{\text{Rabi}} &= \frac{\omega_j}{2}\hat{\sigma}^z + \sum_n \omega_n \hat{a}_n^\dagger \hat{a}_n \\ &- \sum_n g_n (\hat{a}_n - \hat{a}_n^\dagger)(\hat{\sigma}^- - \hat{\sigma}^+).\end{aligned}\quad (49)$$

In the rotating wave approximation, Eq. (49) transforms into the multimode Jaynes-Cummings Hamiltonian

$$\hat{\mathcal{H}}_{\text{JC}} = \frac{\omega_j}{2}\hat{\sigma}^z + \sum_n \omega_n \hat{a}_n^\dagger \hat{a}_n + \sum_n g_n (\hat{\sigma}^+ \hat{a}_n + \hat{\sigma}^- \hat{a}_n^\dagger) \quad (50)$$

used in the main text. Analytic results can be found for the Purcell decay rate and the Lamb shift in the dispersive limit where $g_n \ll |\omega_j - \omega_n|$ [10]. In a Lindblad calculation, resonator losses are included by a Bloch-Redfield approach through the Master equation for the reduced density matrix of the resonator and qubit degrees of freedom $\dot{\rho} = -i[\hat{\mathcal{H}}_{\text{JC}}, \rho] + \frac{\kappa_n}{2}(2\hat{a}_n\rho\hat{a}_n^\dagger - \{\hat{\rho}, \hat{a}_n^\dagger\hat{a}_n\})$, where κ_n can be replaced from the solutions to Eq. (44). The second approach treats the nonlinearity as a weak perturbation and is explained in the next section.

IV. WEAKLY NONLINEAR TRANSMON

By keeping the lowest order nonlinearity (Kerr terms which are quartic in the transmon quadrature), the

Hamiltonian can be rewritten in a new basis that diagonalizes the quadratic part as

$$\begin{aligned}\hat{\mathcal{H}}_{\text{sys}} &\equiv \frac{\beta_j}{4} \left(\hat{\mathcal{X}}_j^2 + \hat{\mathcal{Y}}_j^2 \right) + \sum_n \frac{\beta_n}{4} \left(\hat{\mathcal{X}}_n^2 + \hat{\mathcal{Y}}_n^2 \right) \\ &- \frac{\epsilon\omega_j}{8} \left(u_j \hat{\mathcal{X}}_j + \sum_n u_n \hat{\mathcal{X}}_n \right)^4,\end{aligned}\quad (51)$$

where $\epsilon \equiv \sqrt{2}\epsilon/6$ and $\beta_{j,n}$ are the hybridized frequencies and $u_{j,n}$ are the hybridization coefficients found from diagonalization as $\hat{\mathcal{X}}_j = u_j \hat{\mathcal{X}}_j + \sum_n u_n \hat{\mathcal{X}}_n$.

The Heisenberg equations of motion become a set of coupled quantum Duffing equations

$$\begin{aligned}\ddot{\hat{\mathcal{X}}}_l(t) + \beta_l^2 \left\{ \hat{\mathcal{X}}_l(t) - \varepsilon_l \left[u_j \hat{\mathcal{X}}_j(t) + \sum_n u_n \hat{\mathcal{X}}_n(t) \right]^3 \right\} &= 0,\end{aligned}\quad (52)$$

where $\varepsilon_l \equiv \frac{\omega_j}{\beta_l} u_l \epsilon$ for $l \equiv j, n$. Up to lowest order in the perturbation [19], we find an operator renormalization of $\hat{\beta}_j$

$$\hat{\beta}_j = \beta_j - \frac{3\epsilon}{2}\omega_j \left[u_j^4 \hat{\mathcal{H}}_j(0) + \sum_n u_j^2 u_n^2 \hat{\mathcal{H}}_n(0) \right], \quad (53a)$$

and of $\hat{\beta}_n$ as

$$\begin{aligned}\hat{\beta}_n &= \beta_n - \frac{3\epsilon}{2}\omega_j \left[u_n^4 \hat{\mathcal{H}}_n(0) + u_n^2 u_j^2 \hat{\mathcal{H}}_j(0) \right. \\ &\quad \left. + \sum_{m \neq n} u_n^2 u_m^2 \hat{\mathcal{H}}_m(0) \right],\end{aligned}\quad (53b)$$

where $\bar{\mathcal{H}}_l(0) \equiv \frac{1}{4}[\hat{\mathcal{X}}_l^2(0) + \hat{\mathcal{Y}}_l^2(0)]$ for $l \equiv j, n$. In the main text (Eq. (10)), the bar notation is dropped. The lowest order MSPT solution for the qubit quadrature becomes, in terms of renormalized frequencies $\hat{\beta}_{j,n}$, [19]

$$\begin{aligned}\hat{\mathcal{X}}_j^{(0)}(t) &= u_j \frac{\hat{a}_j(0)e^{-i\hat{\beta}_j t} + e^{-i\hat{\beta}_j t}\hat{a}_j(0)}{2 \cos \left(\frac{3\omega_j}{4} u_j^4 \epsilon t \right)} + \text{H.c.} \\ &+ \sum_n \left[u_n \frac{\hat{a}_n(0)e^{-i\hat{\beta}_n t} + e^{-i\hat{\beta}_n t}\hat{a}_n(0)}{2 \cos \left(\frac{3\omega_j}{4} u_n^4 \epsilon t \right)} + \text{H.c.} \right].\end{aligned}\quad (54)$$

This equation takes into account corrections up to $\mathcal{O}(\epsilon)$ in frequencies. To extract these corrections, we must evaluate the expectation value with respect to the initial density matrix. We chose $\hat{\rho} = |\Psi\rangle_j \langle \Psi|_j \otimes |0\rangle_{\text{ph}} \langle 0|_{\text{ph}}$ with $|\Psi\rangle_j = (|0\rangle_j + |1\rangle_j)/\sqrt{2}$. The correction to the transmon like frequency is obtained from the Fourier components of $\langle \hat{\mathcal{X}}_j(t) \rangle$. This is the correction plotted in Fig. 3 of the main text.

V. ASYMPTOTIC BEHAVIOR OF LIGHT-MATTER COUPLING

In this section we find the asymptotic behavior of the eigenfrequencies ω_n and eigenmodes $\tilde{\varphi}_n(x)$ of the resonator discussed in the main text. This provides an analytical understanding of the high frequency suppression in the light-matter coupling $g_n \propto \sqrt{\omega_n} \tilde{\varphi}_n(x_0)$.

To point out the origin of the suppression that arise from a nonzero χ_s , let us consider the closed resonator ($\chi_{R,L} = 0$) case. Consider the special case of $x_0 = 0^+$ first. This is of experimental interest in order to achieve the maximum coupling to all modes of a resonator. Then, the transcendental Eq. (34) simplifies to

$$\sin(\omega_n) + \chi_s \omega_n \cos(\omega_n) = 0, \quad (55)$$

which can be rewritten as

$$\tan(\omega_n) = -\chi_s \omega_n. \quad (56)$$

The large ω_n solution for $\chi_s \neq 0$ is then obtained

$$\lim_{n \rightarrow \infty} \omega_n = n\pi - \frac{\pi}{2}, \quad (57)$$

which is independent of the value for χ_s . This implies that the effect of a nonzero χ_s on ω_n is a total shift $\pi/2$ (half of the free spectral range) in comparison with the case $\chi_s = 0$. Substituting $x_0 = 0^+$ in Eq. (35), the normalization factor \mathcal{N}_n is found via Eq. (36) as

$$\int_0^1 dx \cos^2[\omega_n(1-x)] + \chi_s \cos^2(\omega_n) = \frac{1}{\mathcal{N}_n^2}, \quad (58)$$

which gives

$$\mathcal{N}_n = \frac{\sqrt{2}}{\sqrt{1 + \chi_s \cos^2(\omega_n)}}. \quad (59)$$

Therefore the eigenmode is found as

$$\tilde{\varphi}_n(x_0 = 0^+) = \frac{\sqrt{2} \cos(\omega_n)}{\sqrt{1 + \chi_s \cos^2(\omega_n)}}. \quad (60)$$

Using the trigonometric identity

$$\cos^2(\omega_n) = \frac{1}{1 + \tan^2(\omega_n)} \quad (61)$$

and Eq. (56) we can rewrite Eq. (60) as

$$\tilde{\varphi}_n(x_0 = 0^+) = \frac{\sqrt{2}}{\sqrt{1 + \chi_s + \chi_s^2 \omega_n^2}}, \quad (62)$$

which now provides the algebraic dependence of $\tilde{\varphi}_n(x_0)$ on ω_n . According to Eq. (62), for large enough ω_n ($\chi_s \omega_n \gg 1 + \chi_s$), we find

$$\tilde{\varphi}_n(x_0) \sim \frac{1}{\omega_n}, \quad (63)$$

where the symbol \sim represents asymptotic equivalence. This imposes a natural cut-off on the light matter coupling for $n \rightarrow \infty$, since

$$g_n \propto \sqrt{\omega_n} \tilde{\varphi}_n(x_0) \sim \frac{1}{\sqrt{\omega_n}}. \quad (64)$$

Next, we would like to find the asymptotic behavior of ω_n and $\tilde{\varphi}_n(x_0)$ for a general x_0 . In order to bring Eq. (34) into a similar form to Eq. (56), we first replace $\sin(\omega_n) = \sin[\omega_n x_0 + \omega_n(1-x_0)]$ and then divide by $\cos(\omega_n x_0) \cos[\omega_n(1-x_0)]$ to obtain

$$\tan(\omega_n x_0) + \tan[\omega_n(1-x_0)] = -\chi_s \omega_n. \quad (65)$$

Next, the normalization factor \mathcal{N}_n is found from Eq. (36) as

$$\mathcal{N}_n = \frac{\sqrt{2}}{\sqrt{x_0 \cos^2[\omega_n(1-x_0)] + (1-x_0) \cos^2(\omega_n x_0) + \chi_s \cos^2[\omega_n(1-x_0)] \cos^2(\omega_n x_0)}}, \quad (66)$$

Plugging this into Eq. (35) we find

$$\tilde{\varphi}_n(x_0) = \frac{\sqrt{2}}{\sqrt{1 + \chi_s + x_0 \tan^2(\omega_n x_0) + (1-x_0) \tan^2[\omega_n(1-x_0)]}} \quad (67)$$

Equations (65) and (67) provide the asymptotic behavior of ω_n , $\tilde{\varphi}_n(x_0)$ and g_n for a general x_0 .

VI. CHARACTERISTIC FUNCTION $D_j(s)$ AND ITS CONVERGENCE

In this section we derive the expression for the characteristic function $D_j(s)$ and compare its convergence in

number of resonator modes with and without the modification we found for g_n .

Consider the Heisenberg-Langevin equations of motion corresponding to Hamiltonian (47) in the linear regime ($\epsilon = 0$) for $\hat{\mathcal{X}}_{j,n}(t)$ as

$$(d_t^2 + \omega_j^2) \hat{\mathcal{X}}_j(t) = - \sum_n 2g_n \omega_n \hat{\mathcal{X}}_n(t), \quad (68a)$$

$$(d_t^2 + 2\kappa_n d_t + \omega_n^2) \hat{\mathcal{X}}_n(t) = -2g_n \omega_j \hat{\mathcal{X}}_j(t) - \hat{f}_n(t), \quad (68b)$$

where κ_n and \hat{f}_n are the decay rate and noise operator coming from coupling to the waveguide degrees of freedom [37].

Equations (68a-68b) are linear constant coefficient ODEs and can be solved exactly via the unilateral Laplace transform

$$\tilde{h}(s) = \int_0^\infty dt h(t) e^{-st}. \quad (69)$$

Taking the Laplace transform of Eqs. (68a-68b) we obtain

$$(s^2 + \omega_j^2) \hat{\mathcal{X}}_j(s) + \sum_n 2g_n \omega_n \hat{\mathcal{X}}_n(s) = s \hat{\mathcal{X}}_j(0) + \hat{\mathcal{X}}_j(0), \quad (70a)$$

$$(s^2 + 2\kappa_n s + \omega_n^2) \hat{\mathcal{X}}_n(s) + 2g_n \omega_j \hat{\mathcal{X}}_j(s) = (s + 2\kappa_n) \hat{\mathcal{X}}_n(0) + \hat{\mathcal{X}}_n(0) + \hat{f}(s). \quad (70b)$$

The solution for $\hat{\mathcal{X}}_j(s)$ then reads

$$\hat{\mathcal{X}}_j(s) = \frac{\hat{N}_j(s)}{D_j(s)}, \quad (71)$$

where the numerator

$$\begin{aligned} \hat{N}_j(s) &= s \hat{\mathcal{X}}_j(0) + \hat{\mathcal{X}}_j(0) \\ &- \sum_n \frac{2g_n \omega_n [(s + 2\kappa_n) \hat{\mathcal{X}}_n(0) + \hat{\mathcal{X}}_n(0) - \hat{f}_n(s)]}{s^2 + 2\kappa_n s + \omega_n^2}, \end{aligned} \quad (72)$$

contains the operator initial conditions and the denominator

$$D_j(s) \equiv s^2 + \omega_j^2 - \sum_n \frac{4g_n^2 \omega_j \omega_n}{s^2 + 2\kappa_n s + \omega_n^2}. \quad (73)$$

is the characteristic function whose roots give the hybridized poles of the full system. Therefore, we can represent $D_j(s)$ as

$$D_j(s) = (s - p_j)(s - p_j^*) \prod_n \frac{(s - p_n)(s - p_n^*)}{(s - z_n)(s - z_n^*)}, \quad (74)$$

where $p_{j,n} \equiv -\alpha_{j,n} - i\beta_{j,n}$ stand for the transmon-like and the n th resonator-like poles, respectively. Furthermore, $z_n \equiv -\kappa_n - i\sqrt{\omega_n^2 - \kappa_n^2}$ is the n th bare non-Hermitian resonator mode. The notation (p for poles and z for zeros) is chosen based on $1/D_j(s)$ that appears in the Laplace solution (71).

In order to compute the hybridized poles in practice, we need to truncate the number of resonator modes in $D_j(s)$. This truncation is only justified if the function $D_j(s)$ converges as we include more and more modes. First, note that without the correction give by χ_s this sum is divergent, since $g_n \sim \sqrt{\omega_n} \sim \sqrt{n}$ and for a fixed s we obtain

$$\frac{4g_n^2 \omega_j \omega_n}{s^2 + 2\kappa_n s + \omega_n^2} \sim \frac{\omega_n^2}{\omega_n^2} \sim 1. \quad (75)$$

Hence, the series is divergent. On the other hand, we found that for a non-zero χ_s , $g_n \sim 1/\sqrt{\omega_n} \sim 1/\sqrt{n}$. Therefore we find

$$\frac{4g_n^2 \omega_j \omega_n}{s^2 + 2\kappa_n s + \omega_n^2} \sim \frac{1}{\omega_n^2} \sim \frac{1}{n^2}, \quad (76)$$

and the series becomes convergent. In writing Eq. (76), we used the fact that $\omega_n \sim n$ and κ_n has a sublinear asymptotic behavior found numerically.

[1] D. Kleppner, Phys. Rev. Lett. **47**, 233 (1981).
[2] P. Goy, J. M. Raimond, M. Gross, and S. Haroche, Phys. Rev. Lett. **50**, 1903 (1983).
[3] R. G. Hulet, E. S. Hilfer, and D. Kleppner, Phys. Rev. Lett. **55**, 2137 (1985).
[4] W. Jhe, A. Anderson, E. A. Hinds, D. Meschede, L. Moi, and S. Haroche, Phys. Rev. Lett. **58**, 666 (1987).
[5] E. M. Purcell, H. C. Torrey, and R. V. Pound, Phys. Rev. **69**, 37 (1946).
[6] W. E. Lamb Jr and R. C. Retherford, Physical Review **72**, 241 (1947).
[7] A. Fragner, M. Göppl, J. Fink, M. Baur, R. Bianchetti, P. Leek, A. Blais, and A. Wallraff, Science **322**, 1357 (2008).
[8] A. A. Houck, J. A. Schreier, B. R. Johnson, J. M. Chow, J. Koch, J. M. Gambetta, D. I. Schuster, L. Frunzio,

M. H. Devoret, S. M. Girvin, and R. J. Schoelkopf, Phys. Rev. Lett. **101**, 080502 (2008).

[9] S. E. Nigg, H. Paik, B. Vlastakis, G. Kirchmair, S. Shankar, L. Frunzio, M. H. Devoret, R. J. Schoelkopf, and S. M. Girvin, Phys. Rev. Lett. **108**, 240502 (2012).

[10] M. Boissonneault, J. M. Gambetta, and A. Blais, Phys. Rev. A **79**, 013819 (2009).

[11] S. Filipp, M. Göppl, J. M. Fink, M. Baur, R. Bianchetti, L. Steffen, and A. Wallraff, Phys. Rev. A **83**, 063827 (2011).

[12] M. H. Devoret, in *Les Houches, Session LXIII*, Vol. 7, edited by S. Reynaud, E. Giacobino, and J. Zinn-Justin (Elsevier Science, 1997) pp. 351–386.

[13] J. Koch, T. M. Yu, J. Gambetta, A. A. Houck, D. I. Schuster, J. Majer, A. Blais, M. H. Devoret, S. M. Girvin, and R. J. Schoelkopf, Phys. Rev. A **76**, 042319 (2007).

[14] W. E. Lamb, R. R. Schlicher, and M. O. Scully, Phys. Rev. A **36**, 2763 (1987).

[15] M. Devoret, B. Huard, R. Schoelkopf, and L. F. Cugliandolo, eds., “*Quantum Machines: Measurement and Control of Engineered Quantum Systems: Lecture Notes of the Les Houches Summer School: Volume 96, July 2011*” (Lecture Notes of the Les Houches Summer School 96, 2014).

[16] M. Malekakhlagh, A. Petrescu, and H. E. Türeci, *Supplementary Material*.

[17] M. Malekakhlagh and H. E. Türeci, Phys. Rev. A **93**, 012120 (2016).

[18] P. W. Milonni, “*The quantum vacuum: an introduction to quantum electrodynamics*” (Academic press, 2013).

[19] M. Malekakhlagh, A. Petrescu, and H. E. Türeci, Phys. Rev. A **94**, 063848 (2016).

[20] J. Bourassa, F. Beaudoin, J. M. Gambetta, and A. Blais, Phys. Rev. A **86**, 013814 (2012).

[21] The power law dependence of κ_n and g_n , albeit universal with respect to χ_s , are specific to the chosen circuit topology.

[22] A. Caldeira and A. Leggett, Annals of Physics **149**, 374 (1983).

[23] A. J. Leggett, Phys. Rev. B **30**, 1208 (1984).

[24] F. Schwabl and W. Thirring, “Quantum theory of laser radiation,” in *Ergebnisse der exakten Naturwissenschaften* (Springer Berlin Heidelberg, Berlin, Heidelberg, 1964) pp. 219–242.

[25] F. C. Khanna, A. P. C. Malbouisson, J. Malbouisson, and A. E. Santana, *Thermal quantum field theory: algebraic aspects and applications* (World Scientific Books, 2009).

[26] C. M. Bender and S. A. Orszag, “*Advanced mathematical methods for scientists and engineers*” (Springer Science & Business Media, 1999).

[27] C. M. Bender and L. M. A. Bettencourt, Phys. Rev. Lett. **77**, 4114 (1996).

[28] B. Johnson, M. Reed, A. Houck, D. Schuster, L. S. Bishop, E. Ginossar, J. Gambetta, L. DiCarlo, L. Frunzio, S. M. Girvin, and R. J. Schoelkopf, Nature Physics **6**, 663 (2010).

[29] M. F. Gely, A. Parra-Rodriguez, D. Bothner, Y. M. Blanter, S. J. Bosman, E. Solano, and G. A. Steele, arXiv preprint arXiv:1701.05095 (2017).

[30] L. S. Bishop, arXiv:1007.3520 [cond-mat, physics:quant-ph] (2010).

[31] A. A. Clerk, M. H. Devoret, S. M. Girvin, F. Marquardt, and R. J. Schoelkopf, Rev. Mod. Phys. **82**, 1155 (2010).

[32] P. Morse and H. Feshbach, “*Methods of theoretical physics*” (McGraw-Hill, 1953).

[33] E. N. Economou, “*Green’s functions in quantum physics*”, Vol. 3 (Springer, 1984).

[34] S. Hassani, “*Mathematical physics: a modern introduction to its foundations*” (Springer Science & Business Media, 2013).

[35] H. E. Türeci, A. D. Stone, and B. Collier, Phys. Rev. A **74**, 043822 (2006).

[36] H. E. Türeci, L. Ge, S. Rotter, and A. D. Stone, Science **320**, 643 (2008).

[37] I. R. Senitzky, Phys. Rev. **119**, 670 (1960).